FEBS Letters 581 (2007) 413–420

Dynamic simulation of an in vitro multi-enzyme system

Nobuyoshi Ishii[a,b], Yoshihiro Suga[a], Akiko Hagiya[a], Hisami Watanabe[a], Hirotada Mori[a,c], Masataka Yoshino[a,d], Masaru Tomita[a,b,*]

[a] *Institute for Advanced Biosciences, Keio University, Tsuruoka 997-0035, Japan*
[b] *Systems Biology Program, Graduate School of Media and Governance, Keio University, Fujisawa 252-8520, Japan*
[c] *Graduate School of Biological Sciences, Nara Institute of Science and Technology, Ikoma 630-0192, Japan*
[d] *Department of Biochemistry, Aichi Medical University School of Medicine, Nagakute 480-1195, Japan*

Received 7 August 2006; revised 23 November 2006; accepted 25 December 2006

Available online 12 January 2007

Edited by Robert B. Russell

Abstract Parameters often are tuned with metabolite concentration time series data to build a dynamic model of metabolism. However, such tuning may reduce the extrapolation ability (generalization capability) of the model. In this study, we determined detailed kinetic parameters of three purified *Escherichia coli* glycolytic enzymes using the initial velocity method for individual enzymes; i.e., the parameters were determined independently from metabolite concentration time series data. The metabolite concentration time series calculated by the model using the parameters matched the experimental data obtained in an actual multi-enzyme system consisting of the three purified *E. coli* glycolytic enzymes. Thus, the results indicate that kinetic parameters can be determined without using an undesirable tuning process.

Keywords: Dynamic simulation; Mathematical model; Enzyme kinetics; Metabolism; Glycolysis

1. Introduction

Dynamic simulation is a powerful method for analyzing the complex behavior of metabolic systems, which involve many enzymatic reactions. A detailed dynamic model of a metabolic system usually is constructed using several enzymatic rate equations, such as the Michaelis–Menten equation, to which kinetic parameters collected from the literature reports are applied. However, in most cases, kinetic models constructed from reported literature values inadequately simulate the metabolism of living cells [1]. One reason for this is the difference in the in vitro and in vivo kinetic parameters [1]. Optimal conditions applied to activity measurements of an enzyme usually are not similar to intracellular conditions [2]. Moreover, special phenomena, such as protein–protein interactions [3] or metabolic channeling [4], may occur in actual cells.

Parameter tuning by applying experimental results, usually data from time series of metabolite concentrations, is performed to match models to experimental data [5–7]. The tuning processes can involve non-physical (empirical) power-law equations such as S-System or generalized mass action (GMA) [8,9], or non-mechanistic models [10] (lumped model [11], unstructured model [12]). These approaches reproduce metabolite time series data used for tuning [10,13,14].

However, the tuned parameters are not always unique and may lose physicochemical meaning, or may produce parameters with unclear physiological meaning. For example, the Michaelis–Menten constant (K_m) has a physicochemical meaning of "the substrate concentration that indicates one-half maximum velocity of an enzyme reaction". However, once a model consisting of Michaelis–Menten equations is converted to an S-system or a GMA model, tuned coefficients in the converted rate equations no longer have such specific meanings.

Furthermore, a model optimized for matching time series data sets may not be predictive under other conditions. One important purpose of simulation studies is to predict responses of the system under unexamined conditions. To achieve this, physical (theoretical) and mechanistic models using parameters obtained independently from particular metabolite time series data are needed to allow extrapolation. However, no studies have reported mechanistic models constructed using enzyme kinetic equations with physiologically meaningful parameter sets, which accurately estimate the behavior of a multi-enzyme system.

Here, we validate a dynamic model consisting of individual enzyme kinetic equations using an in vitro system without the difficulties inherent in in vivo systems. We purified three glycolysis enzymes in *Escherichia coli* and determined their individual kinetic parameters under identical conditions. Subsequently, a multi-enzyme system consisting of the three purified enzymes was constructed under the same conditions used for measurements of the kinetic parameters. A time series of metabolites in the multi-enzyme system was obtained and compared with calculated values from a dynamic simulation using kinetic parameters measured in each single-enzyme system. Inactivation of each enzyme was experimentally evaluated and incorporated in the simulation.

2. Materials and methods

2.1. Expression and purification of protein

The *E. coli* strains included in the ASKA clone library [15], which is based on *E. coli* K-12 strain AG1 [*recA*1 *endA*1 *gyrA*96 *thi*-1 *hsdR*17

*Corresponding author. Fax: +81 235 29 0809.
E-mail address: mt@sfc.keio.ac.jp (M. Tomita).

Abbreviations: ALD, aldolase (EC 4.1.2.13); DTT, dithiothreitol; F6P, fructose-6-phosphate; FDP, fructose-1,6-diphosphate; G3PDH, glycerol-3-phosphate dehydrogenase (EC 1.1.1.8); G6P, glucose-6-phosphate; G6PDH, glucose-6-phosphate dehydrogenase (EC 1.1.1.49); Glk, glucokinase (EC 2.7.1.2); IPTG, isopropyl-β-D-thiogalactopyranoside; MOPS, 3-morpholinopropanesulfonic acid; Pfk, phosphofructokinase (EC 2.7.1.11); Pgi, phosphoglucoisomerase (EC 5.3.1.9); TIM, triose phosphate isomerase (EC 5.3.1.1)

0014-5793/$32.00
doi:10.1016/j.febslet.2006.12.049

($r_K^- m_K^+$) *supE*44 *relA*1], were used. Cells producing histidine-tagged protein (Glucokinase (EC 2.7.1.2) (Glk), phosphoglucoisomerase (EC 5.3.1.9) (Pgi), and PfkA) from the ASKA clone were grown at 37 °C in 200 ml of LB medium supplemented with 50 μg/ml chloramphenicol to OD_{600} 0.5. Samples were obtained 2 h after addition of 0.1 mM isopropyl-β-D-thiogalactopyranoside (IPTG). The cells were collected by centrifugation (6000 r.p.m., 5 min at 4 °C) and resuspended in 10 ml of cold buffer I [50 mM sodium phosphate (pH 7.0), 200 mM NaCl, Protease inhibitor (Complete Mini EDTA-Free, Roche Diagnostics, Basel, Switzerland)]. All subsequent manipulations were conducted at 4 °C. Crude cell extracts were obtained by sonication [10 × 5 s, level 3, ultrasonic disruptor UD-201 (TOMY, Tokyo, Japan)] and centrifugation (9000 r.p.m., 20 min at 4 °C). Crude cell extracts were loaded onto a 2-ml nickel (Ni^{2+}) column [prepared according to manufacturer's instructions (QIAGEN) and equilibrated with buffer I]. Affinity chromatography of the extracts was performed at 4 °C. Loaded columns were washed three times with 7 ml of buffer II (buffer I containing 20 mM imidazole) and proteins were eluted with buffer III (buffer I containing 250 mM imidazole). Finally, enzymes were stored in buffer III containing 20% glycerol at −20 °C until use. Their concentration then was measured using BCA protein assay reagent (Pierce Chemicals).

2.2. Kinetic rate equations

Kinetic rate equations are shown in Table 1. The rate equation for Glk is shown in this study (see Section 3.1). Other equations were taken from the literature reports.

2.3. Kinetic analysis

All enzyme kinetic assays were conducted at 37 °C in 100 mM 3-morpholinopropanesulfonic acid (MOPS) buffer (pH 7.2) containing 2 mM dithiothreitol (DTT). Enzyme was added to a concentration between 0.001 μM and 5 μM. Glk activity was measured using 8 U/ml Glucose-6-phosphate dehydrogenase (EC 1.1.1.49) (G6PDH), 1 mM NADP, 20 mM $MgCl_2$, and various concentrations of glucose and ATP. Pgi forward reaction activity (G6P to F6P) was measured using 1.8 U/ml aldolase (EC 4.1.2.13) (ALD), 31 U/ml Glycerol-3-phosphate dehydrogenase (EC 1.1.1.8) (G3PDH), 90 U/ml triose phosphate isomerase (EC 5.3.1.1) (TIM), 12 U/ml phosphofructokinase (EC 2.7.1.11) (Pfk), 0.2 mM NADH, 5 mM $MgCl_2$, and various concentrations of Glucose-6-phosphate (G6P). Pgi reverse reaction activity (F6P to G6P) was measured using 0.1 mM NADP, 1.8 U/ml G6PDH, and various concentrations of fructose-6-phosphate (F6P). PfkA activity was measured using 0.1 mM NADH, 5 mM $MgCl_2$, 1.8 U/ml ALD, 31 U/ml G3PDH, 90 U/ml TIM, and various concentrations of ATP and F6P. For all assays, absorbance at 340 nm (A_{340}) was recorded and initial velocities calculated from the slope of the lines. Kinetic constants were calculated from substrate concentrations and corresponding initial velocities by the Levenberg–Marquardt nonlinear least squares algorithm [16]. One unit of Glk activity was defined as the amount of enzyme needed to catalyze the phosphorylation of 1 μmol glucose in one minute. One unit of forward reaction of Pgi activity was defined as the amount of enzyme per minute needed to catalyze the isomerization of G6P. One unit of reverse reaction of Pgi activity was defined as the amount of enzyme per minute needed to catalyze the isomerization of F6P. One unit of PfkA activity was defined as the amount of enzyme needed to catalyze the phosphorylation of 1 μmol F6P per minute. One unit of G6PDH, ALD, G3PDH, or TIM was defined according to manufacturer's instructions (Roche Diagnostics).

2.4. Equilibrium constant of Pgi forward reaction

An amount of 0.05 μM Pgi was added to 100 mM MOPS buffer (pH 7.2) containing 1 mM G6P and 2 mM DTT, and the reaction solution incubated at 37 °C. Samples taken at predetermined time points were mixed with a 4-fold volume of methanol at 0 °C. The inactivated Pgi was removed by filtration through a centrifugal filter (Biomax, 5000 molecular weight cutoff, Millipore). The filtrate was freeze-dried immediately and dissolved in water prior to measuring the metabolite concentration. The equilibrium constant of the Pgi forward reaction was calculated using concentrations of G6P and F6P once they had achieved a constant value.

2.5. Enzyme inactivation analysis

Activity of an enzyme was measured, followed by addition of 0.05 μM enzyme to 100 mM MOPS buffer (pH 7.2) containing various concentrations of DTT, and the solution was incubated at 37 °C for 1 h. Then, 0.2 ml of the incubated solution was removed and its activity measured immediately. An activity persistence ratio of the enzyme examined was obtained by dividing the activity after incubation by the activity measured before incubation.

2.6. Time series of metabolite concentration in a multi-enzyme system

The metabolic network diagram of the multi-enzyme system examined in this study is shown in Fig. 1. An amount of 1 mM glucose was added to 100 mM MOPS buffer (pH 7.2) containing 0.05 μM Glk, 0.05 μM Pgi, 0.05 μM PfkA, 2 mM ATP, 10 mM $MgCl_2$, and 2 mM DTT, and the reaction solution incubated at 37 °C. Samples were removed at predetermined time points and processed according to the procedure outlined in Section 2.4.

2.7. Measurement of metabolite concentrations

A sample was added to 100 mM MOPS buffer (pH 7.2) containing 0.1 mM NADH, 20 mM $MgCl_2$, 5 mM ATP, and 2 mM DTT (I), and maintained at 37 °C. Then, 1.8 U/ml ALD, 31 U/ml G3PDH,

Table 1
Kinetic rate equations [v, specific activity (U/mg); V_{max}, maximum velocity (U/mg); C, concentration (mM); K_m, Michaelis–Menten constant (mM); n, Hill's n]

Enzyme	Reaction	Rate equation	Source
Glk	Glucose + ATP → G6P + ADP (irreversible)	$v = \frac{V_{max} \cdot C_{glucose} \cdot C_{ATP}}{(K_{m,glucose} + C_{glucose}) \cdot (K_{m,ATP} + C_{ATP})}$ (1)	This work
Pgi	G6P ↔ F6P (reversible)	$v = \frac{V_{max} \cdot \left(C_{G6P} - \frac{C_{F6P}}{K_{eq,Pgi}}\right)}{K_{m,G6P} \cdot \left(1 + \frac{C_{F6P}}{K_{m,F6P}}\right) + C_{G6P}}$ (2)	[7]
PfkA	F6P + ATP → FDP + ADP (irreversible)	$v = \frac{V_{max} \cdot C_{F6P}^n \cdot C_{ATP}}{\left(K_{m,F6P}^n + C_{F6P}^n\right) \cdot (K_{m,ATP} + C_{ATP})}$ (3)	[52]

Each suffix for C or K_m denotes corresponding metabolite.

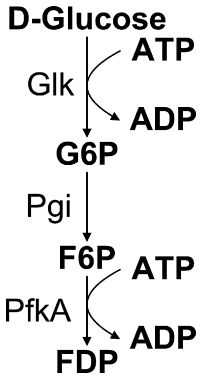

Fig. 1. Schematic diagram of the metabolic network examined in this study.

and 90 U/ml TIM (II), 3 U/ml PfkA (III), 18 U/ml Pgi (IV), and 10 U/ml Glk (V) were added sequentially, and A_{340} was recorded at each step. Concentrations of fructose-1,6-diphosphate (FDP), F6P, G6P, and glucose were calculated from the difference in A_{340} between I and II, II and III, III and IV, and IV and V, respectively. The FDP concentration of each sample was calibrated by the measured value of a known concentration standard solution of FDP treated using the same procedure employed for sample preparation.

2.8. Dynamic simulation

According to Table 1, the ordinary differential equations (ODEs) describing the velocities of metabolite concentration change in the tested system can be expressed as

$$\mathrm{d[Glucose]}/\mathrm{d}t = -v_{\mathrm{Glk}} \quad (4)$$

$$\mathrm{d[G6P]}/\mathrm{d}t = v_{\mathrm{Glk}} - v_{\mathrm{Pgi}} \quad (5)$$

$$\mathrm{d[F6P]}/\mathrm{d}t = v_{\mathrm{Pgi}} - v_{\mathrm{PfkA}} \quad (6)$$

$$\mathrm{d[FDP]}/\mathrm{d}t = v_{\mathrm{PfkA}} \quad (7)$$

$$\mathrm{d[ATP]}/\mathrm{d}t = -v_{\mathrm{Glk}} - v_{\mathrm{PfkA}} \quad (8)$$

$$\mathrm{d[ADP]}/\mathrm{d}t = v_{\mathrm{Glk}} + v_{\mathrm{PfkA}} \quad (9)$$

where t is time (min), v_{Glk} is reaction rate of Glk (mM/min), v_{Pgi} is reaction rate of Pgi (mM/min), and v_{PfkA} is reaction rate of PfkA (mM/min). Dynamic simulations of the multi-enzyme system based on Eqs. (4)–(9) were performed using E-Cell 3.1.104 (http://www.e-cell.org/). Initial concentrations of metabolites were set to the values described in Section 2.6. The ODE45 algorithm [17] was employed for numerical integration.

2.9. Parameter tuning with metabolite concentration time series data

Parameter tuning with metabolite concentration time series data obtained in Section 2.6 was performed using the genetic algorithm (GA) [18]. The fitness function used in the GA calculations is

$$f = \frac{\sum_{i=1}^{n_{\mathrm{samplingpoint}}} \sum_{j=1}^{n_{\mathrm{metabolite}}} \left(\frac{C_{\mathrm{data},i,j} - C_{\mathrm{calculated},i,j}}{C_{\mathrm{data},i,j}} \right)^2}{n_{\mathrm{samplingpoint}} \cdot n_{\mathrm{metabolite}}} \quad (10)$$

where f is fitness function, $C_{\mathrm{data},i,j}$ is measured concentration of the jth metabolite at the ith sampling point (mM), $C_{\mathrm{calculated},i,j}$ is calculated concentration of the jth metabolite at the ith sampling point by tuned rate equation parameters (mM), $n_{\mathrm{metabolite}}$ is the number of metabolites, and $n_{\mathrm{sampling\ point}}$ is the number of sampling points. The optimizations were performed using two methods: with a constraint that rate equation parameters should be non-negative, and with no constraint for the parameters. MATLAB Release 2006a (MathWorks) and the Genetic Algorithm and Direct Search Toolbox 2.0.1 (MathWorks) were employed for the optimizations. ODEs with tuned parameters were solved by the same method in Section 2.8. In each GA calculation, the population number was set to 1000. The other GA parameters were set to default values. Each optimal solution was taken after the fitness function converged to a constant value.

3. Results

3.1. Kinetic parameters of each enzyme

Kinetic parameters of enzymes tested and the equilibrium constant of Pgi forward reaction are shown in Table 2. All measurement data are shown in Figs. 1S and 2S in Supplementary material.

The kinetic parameters taken from BRENDA (release 08/2006; http://www.brenda.uni-koeln.de/) [19], one of the most widely known public enzyme databases, also are shown in Table 2. $K_{\mathrm{m,glucose}}$ of Glk, $K_{\mathrm{m,ATP}}$ of Glk, $K_{\mathrm{m,F6P}}$ of Pgi, and $V_{\max}$ of PfkA displayed good agreement with some of the database values. However, for $K_{\mathrm{m,glucose}}$ of Glk and $K_{\mathrm{m,ATP}}$ of Glk, some of the database values did not match the values in this study, and other parameters in the database differed significantly from our values. The kinetic parameters may vary depending on the strain used and/or experimental conditions including buffer used, pH, and temperature. Since the data collected in BRENDA were obtained from different strains and under various conditions, and the strains and/or conditions were not always same as those of this study, the parameter differences between this study and the database is not improbable. Furthermore, some parameters required for this study were not found in BRENDA, especially parameters for complex rate equations, such as Hill's n for PfkA. Moreover, although the equilibrium constant for the Pgi reaction is needed to calculate the reversibility of this enzyme reaction, the constant also is not registered in BRENDA. Collecting equilibrium constants is not the purpose of BRENDA, and equilibrium constants can be calculated from thermodynamic data [20]. However, actual equilibrium constants depend on the solution composition, therefore experimentally measured values are actually required. This information suggests that current public enzyme databases are not always sufficient for building an accurate dynamic model of metabolism, thus parameter-determining experiments performed in under uniform conditions are needed.

For the Pgi, Eq. (2) (Table 1) was obtained from the *E. coli* model constructed by Chassagnole et al., who reported the estimated in vivo parameters of Pgi in their study [7]: $K_{\mathrm{m,G6P}}$, $K_{\mathrm{m,F6P}}$, $K_{\mathrm{eq,Pgi}}$ were 2.9 mM, 0.27 mM, and 0.17, respectively. These values were similar to our values (Table 2), and variation in $K_{\mathrm{eq,Pgi}}$ might reflect the difference in chemical composition between in vivo and in vitro.

No rate equation for Glk from *E. coli* has been reported in the literature, so the reaction rate equation of the Glk was determined for this study. Double-reciprocal plots [21] of Glk with two substrate concentrations are shown in Fig. 2. The slope of the plots of 1/glucose versus 1/v at fixed ATP concentration decreased with an increase in ATP concentration, and all double-reciprocal plots crossed at a point within the negative area of the 1/glucose axis. From these results, the reaction mechanism of Glk can be estimated as rapid equilibrium Random Bi–Bi [21] or Ordered Bi–Bi with steady-state assumption [21]. Since the plot crossing point occurred on the 1/glucose axis, a Random B–Bi reaction mechanism would give an interaction coefficient between the two substrates of 1 [21]; if the reaction mechanism is Ordered Bi–Bi, the dissociation constant for first-binding substrate is almost equal to K_{m} for the first-binding substrate [21]. The true reaction mechanism, Random Bi–Bi or Ordered Bi–Bi, cannot be determined by the initial velocity analysis [21]. However, since the reaction

Table 2
Kinetic rate equation parameters

Source		This work	BRENDA (release 08/2006)	This work	This work
Method		Initial velocity method		Tuning using metabolite concentration time series data, with a constraint[a]	Tuning using metabolite concentration time series data, without constraint
Enzyme	Parameter	Value			
Glk	V_{max}	255 U/mg	158 U/mg	271 U/mg	204 U/mg
	$K_{m,glucose}$	0.12 mM	0.15 mM, 0.78 mM[b]	0.02 mM	0.35 mM
	$K_{m,ATP}$	0.50 mM	0.50 mM, 3.76 mM[b]	0.00005 mM	−0.50 mM
Pgi	V_{max}	1511 U/mg	N.D.	126 U/mg	142 U/mg
	$K_{m,G6P}$	3.0 mM	N.D.	0.00027 mM	0.0066 mM
	$K_{m,F6P}$	0.16 mM	0.2 mM	3.37 mM	−0.13 mM
	$K_{eq,\ pgi}$	0.30	N.D.	0.39	0.39
PfkA	V_{max}	145 U/mg	184 U/mg[c,d], 102 U/mg[c,e], 263 U/mg, 190 U/mg, 189 U/mg	23 U/mg	18 U/mg
	$K_{m,F6P}$	0.46 mM	0.096 mM[f]	0.13 mM	0.10 mM
	$K_{m,ATP}$	0.04 mM	0.10 mM[g], 0.21 mM[h]	0.12 mM	0.04 mM
	n (for F6P)	1.9	N.D.	3.0	3.6

N.D. denotes "no data". All parameters from BRENDA are for *Escherichia coli*. For PfkA data from BRENDA, if pH is specified, only the values examined under conditions similar to this work (pH 7.2) were used.
[a]Parameters should be non-negative.
[b]pH 7.65.
[c]Calculated from turnover number. The molecular weight of PfkA (34834) was obtained from the GenoBase (http://ecoli.naist.jp/GB6/search.jsp).
[d]4: pH 7.2, 30 °C, at 2 mM ATP.
[e]pH 7.2, 30 °C, co-substrate ATP.
[f]pH 7.2, 30 °C, co-substrate gamma-thio-ATP.
[g]pH 7.2, 30 °C.
[h]pH 7.2, 30 °C.

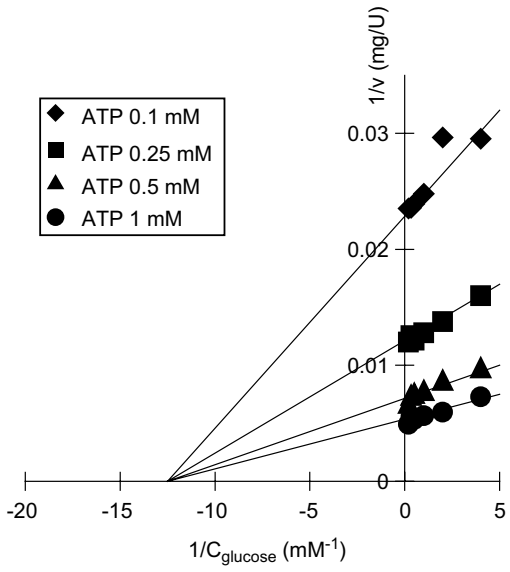

Fig. 2. Double-reciprocal plots of Glk with two substrate concentrations [v is the specific activity of Glk (U/mg); $C_{glucose}$ is glucose concentration (mM)].

rate equations of these two reaction mechanisms can be expressed by the same formula [21], calculating the reaction rates of Glk can be performed without knowledge of the true reaction mechanism. Thus, Eq. (1) (Table 1) was applied to calculate Glk reaction rates. The calculated reaction rates showed good agreement with the measured values shown in Fig. 2 (correlation coefficient = 0.988), verifying the propriety of Eq. (1) (see Fig. 3S in Supplementary material).

3.2. Inactivation of enzymes

In metabolic simulation studies, the kinetic parameters used in a model usually are assumed to be constant during the reaction. For initial velocity determination experiments, this assumption is acceptable because the reaction time is usually very short. However, in experiments reconstituting a portion of metabolic system, long reaction times are sometimes undertaken to observe time-dependent changes in metabolite concentrations. During such prolonged reaction times, maintaining enzyme activity is not always possible in an in vitro system. Thus, for comparison of the experimental data and simulation values, inactivation of each enzyme should be considered.

Significant inactivation of PfkA at 37 °C was observed (Fig. 3, DTT concentration of 0.0 mM), which was suppressed by addition of DTT. Optimal concentration for maintaining PfkA activity was 2.0 mM (Fig. 3). For Glk and Pgi, an activity persistence ratio with 2.0 mM DTT was determined, which revealed that Glk was significantly inactivated (35%). For Pgi, neither the forward nor the reverse reactions were inactivated (106% for forward reaction, 90% for reverse reaction).

Maintaining the activity of PfkA, which has a complex kinetic mechanism, was a priority in this study. For Glk, a time series for inactivation was obtained (Fig. 4). As shown in Fig. 4, the rate equation of Glk inactivation was first-order, with the active and inactive forms of Glk reaching equilibrium. Thus, the rate equation of Glk inactivation can be described using the following:

$$v = k_{Glk,inactivation}\left(C_{Glk,active} - \frac{C_{Glk,inactive}}{K_{eq,Glk,inactivation}}\right) \quad (11)$$

where v is inactivation rate of Glk (μM/min), $k_{Glk,inactivation}$ is the rate constant (min^{-1}), $C_{Glk,active}$ is the active form of Glk

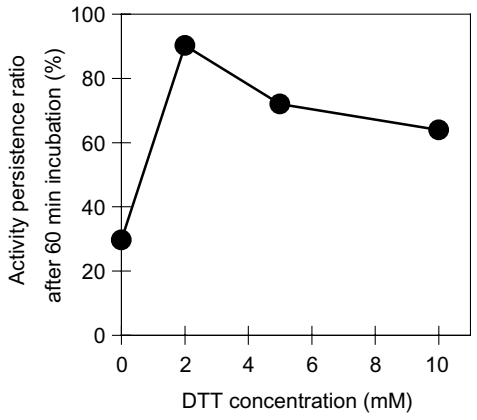

Fig. 3. PfkA activity persistence ratio determined using predetermined concentrations of DTT.

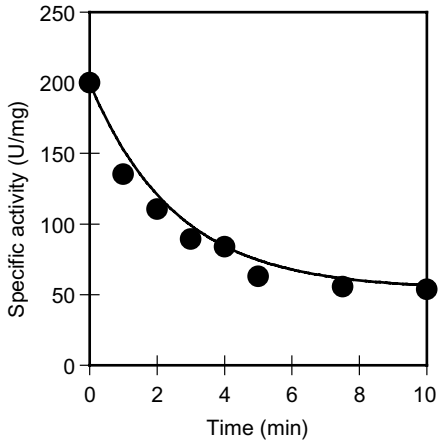

Fig. 4. Inactivation time series of Glk. Closed circles represent experimental data; line indicates values calculated using Eq. (11) with parameters shown in Table 3.

(μM), $C_{Glk,inactive}$ is the inactive form of Glk (μM), and $K_{eq,Glk,inactivation}$ is the equilibrium constant between active and inactive Glk. As shown in Fig. 4, the parameters in Eq. (11) were determined and applied to the following simulation study.

3.3. Comparison of measured values with simulation values

Measured and calculated time series for metabolite concentrations after addition of glucose are shown in Fig. 5. At each sampling point, the sum of measured concentrations of glucose, G6P, F6P, and FDP was approximately 1.0 mM (the initial concentration of glucose), indicating the metabolite concentration assays were performed properly. Chassagnole et al. reported that the steady-state concentrations of G6P, F6P, and FDP in *E. coli* cells grown in a continuous culture (dilution rate = 0.1 h^{-1}) were 3.48 mM, 0.60 mM, and 0.27 mM, respectively [7]. These concentrations were close to the values shown in Fig. 5, indicating our experiment was performed under physiologically meaningful conditions.

As shown in Fig. 5, discrepancies in metabolite concentration between measured and calculated values were sufficiently small. Therefore, the model successfully reproduced the experimental results. Fig. 5 also shows glucose time series estimated data without consideration of Glk inactivation. When Glk inactivation was not incorporated into the calculation, the glucose disappeared too rapidly (ca. 8 min), indicating that the use of Glk inactivation effectively reduced error in the glucose time series estimation.

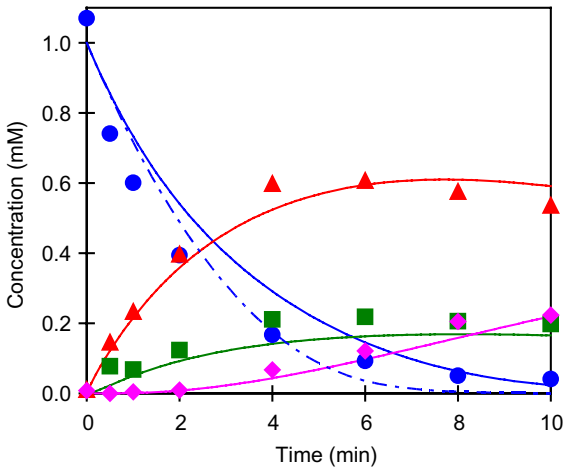

Fig. 5. Comparison of calculated and experimental values of the metabolite concentration time series. Calculations were performed using the parameters obtained from individual enzyme analyses. Blue circles represent glucose (experimental); blue line represents glucose (calculated with consideration of Glk inactivation); blue dotted line represents glucose (calculated without consideration of Glk inactivation); red triangles represent G6P (experimental); red line represents G6P (calculated); green squares represent F6P (experimental); green line indicates F6P (calculated); magenta rhombus indicates FDP (experimental); magenta line represents FDP (calculated).

For PfkA, more complex rate equations than Eq. (3) have been reported. One of the most elaborate mechanistic models is the Monod–Wyman–Changeux model (MWC model) [22] that explains cooperative behavior of an allosteric enzyme. Blangy et al. applied the MWC model to *E. coli* Pfk and determined some parameters experimentally [23]. In the results of Blangy et al., the Hill's n, $K_{m,F6P}$ and V_{max} varied under different concentrations of ADP [23]. In our study, although values for Hill's n, $K_{m,F6P}$ and V_{max} were fixed for PfkA, the time series of substrate (F6P) and product (FDP) for PfkA were successfully reproduced by the model (Fig. 5). This could be predicted, because the increase in ADP causes both activation and inhibition of Pfk activity [23], and so calculations using the fixed parameters accurately approximated the reaction rate change resulting from the mixed effect of activation and inhibition. This may not be true in systems that have a wider range of metabolite concentrations, therefore application of the MWC equation should be considered for precise and predictive simulations.

3.4. Comparison of parameters determined by the initial velocity method for individual enzymes and by tuning with metabolite concentration time series data

In most dynamic models of metabolism designed to reproduce actual experimental data (from both in vivo and in vitro systems), parameter tuning with metabolite concentration time series data has been performed. We also estimated the rate equation parameters in our test system using a popular tuning procedure. As described in Section 2.9, two different tuning methods were used; one optimized with the constraint

Table 3
Inactivation rate equation parameters for Glk

Method	Inactivation experiment	Tuning using metabolite concentration time series data, with a constraint[a]	Tuning using metabolite concentration time series data, without constraint
Parameter	Value		
$k_{Glk,inactivation}$	0.29 min^{-1}	0.46 min^{-1}	0.16 min^{-1}
$K_{eq,Glk,inactivation}$	2.72	57.6	−2.98

[a]Parameters should be non-negative.

of non-negative parameter values, and the other with no constraints. Tables 2 and 3 show the parameters determined by tuning with metabolite concentration time series data. Fig. 6A and B shows the metabolite concentration time series calculated with tuned parameters. The simulations using parameters obtained by tuning with time series data reproduced the metabolite concentration measurements very well (Fig. 6A and B). However, as shown in Tables 2 and 3, the tuned parameters differed significantly from the values determined in the kinetic analysis for the individual enzymes, indicating that use of the tuned parameters is limited to reproduction of the data set employed for the tuning. Moreover, in results obtained from optimization with no parameter constraints, some negative parameters were included. For equilibrium constants or parameters that have the dimension of concentration (mM), such negative values have no physicochemical meaning.

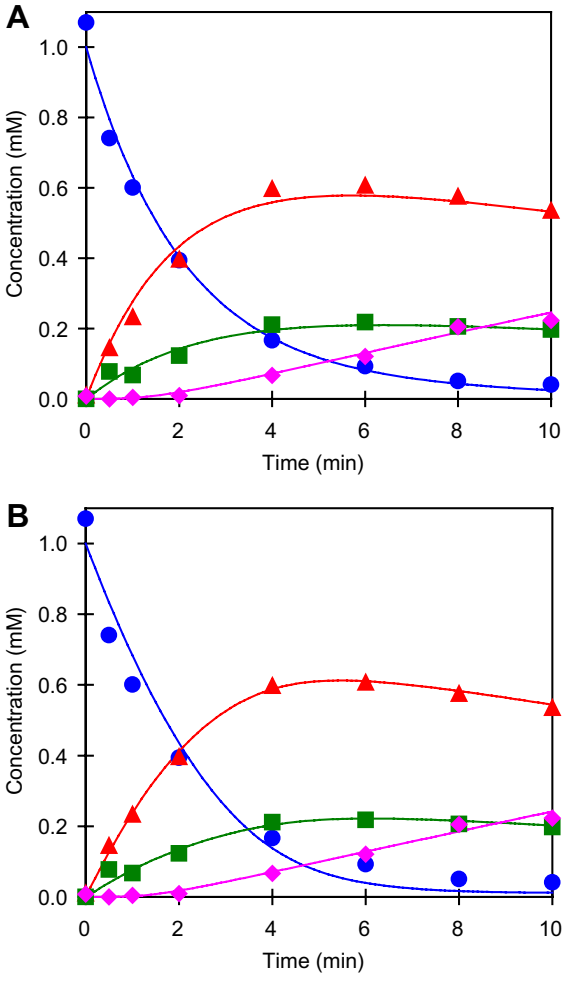

Fig. 6. Comparison of calculated and experimental values of the metabolite concentration time series. Calculations were performed with parameters obtained by tuning with the metabolite concentration time series data. (A) Parameter tuning performed with the constraint that parameters be non-negative. (B) Parameter tuning performed with no constraint. Blue circles represent glucose (experimental); blue line represents glucose (calculated with consideration of Glk inactivation); red triangles represent G6P (experimental); red line represents G6P (calculated); green squares represent F6P (experimental); green line indicates F6P (calculated); magenta rhombus indicates FDP (experimental); magenta line represents FDP (calculated).

4. Discussion

Some pioneering experiments were performed to reconstruct a metabolic pathway in an in vitro system. Scopes studied an artificial glycolytic system reconstituted from purified rabbit and pig muscle glycolytic enzymes [24,25]. Itoh et al. also tested an in vitro glycolytic system consisting of purified *E. coli* enzymes [26]. Cuebas and Schulz reconstituted a β-oxidation system using purified pig heart and beef liver enzymes [27]. These reports provided significant insights into the regulation mechanism of metabolic systems, but included no simulation study. Simultaneously, development of dynamic models that explain the behavior of metabolites in an in vivo system, cell extracts, or an in vitro reconstituted metabolic system have been attempted. Lambeth et al. succeeded in reproducing the dynamic data of phosphocreatine and inorganic phosphate in mouse hind limb muscle measured by nuclear magnetic resonance (NMR) using the glycogenolysis model based on the literature in vitro parameters [28]. Vinnakota et al. augmented the model of Lambeth et al. [28] to deal with pH changes and resulting enzymatic activity alterations [29]. Rizzi et al. constructed a model of yeast carbon metabolism that reproduces time series metabolite data after glucose pulse injection to the culture broth [6]. A model for *E. coli* [7] was created using the strategy proposed by Rizzi et al. [6]. Chassagnole et al. built a model of threonine synthesis in *E. coli* cell extracts [5]. Curien et al. constructed two in vitro systems to validate their kinetic model of methionine and threonine biosynthesis with purified enzymes [30]. All of these models included parameter tuning processes to fit calculated values with time series data of metabolite concentrations or the metabolic flux of the modeled system. However, as shown in Tables 2 and 3, the generalization capability and physicochemical and/or physiological meaning of the parameters may be lost through such tuning manipulations.

Fievet et al. reconstituted a portion of glycolysis using purified enzymes and proposed a non-mechanistic model of the system [10]. Their model included no classical kinetic constants for

individual enzymes. This non-mechanistic approach simplifies identification of model parameters and is sufficient to estimate overall metabolic flux through the modeled system. However, regulatory functions of individual enzymes in a metabolic system cannot be analyzed by such non-mechanistic models.

Fig. 5 shows that, when accurate kinetic parameters are provided, a physical/mechanistic model can simulate the behavior of a real multi-enzyme system without tuning using particular metabolite concentration time series data. These results indicate a generalized living cell metabolic model can be built using parameters determined in an environment that mimics an in vivo system. For this purpose, not only basic physical properties such as temperature and pH, but also other factors that affect enzymatic reactions such as chemical species (containing other proteins that interact with the modeled enzyme), ion strength [31,32], redox balance [33], dimension restriction [34,35], and macromolecular crowding [36–39], may be considered for the in vitro enzyme kinetic analysis method. For example, macromolecular crowding can be reproduced by addition of a polymer such as polyethylene glycol [39] or a globular protein such as hemoglobin [38]. To reconstruct the natural environment for a membrane-bound or a trans-membrane enzyme is very difficult. However, efforts to construct the artificial structure for determining realistic kinetic parameters of membrane proteins continue. Marchal et al. reported a hemi-bilayer membrane system to measure the two-dimensional kinetic parameters of a membrane enzyme, *E. coli* pyruvate oxidase [40]. Since their system is not a complete double layer system, trans-membrane enzymes cannot be incorporated. Wong et al. attempted to reproduce more realistic cellular membrane structures for investigations of trans-membrane proteins, and developed techniques to make new phospholipid bilayer systems [41]. Their bilayer systems are supported on a soft polymer cushion and exhibit more natural fluidity than the previous solid-supported membrane systems. Application of these bilayer systems for evaluation of properties of trans-membrane enzymes remains a challenge.

For chemical species that affect enzyme activities, some important factors may be lost during preparation of an enzyme or an isolated organelle. For instance, Korzeniewski indicated some calmodulin analogous proteins work with calcium ions to activate enzymes in a mitochondrial oxidative phosphorylation system, and these proteins are lost or inactivated during mitochondria preparation [42]. One solution for this problem is the use of an in situ system. Permeabilized cell techniques [43] allow researchers to handle concentrations of specific metabolites in cells while maintaining an intact cytoplasmic environment. Yoshino et al. used permeabilized cells to study the role of AMP deaminase in yeast [44]. The yeast AMP deaminase is deactivated during the purification processes [45], and no method to avoid this degradation has been found. Accordingly, the permeabilized cell method is efficient for determining the true kinetics of the yeast AMP deaminase. Saks et al. summarized the applications of permeabilized cell methods for analysis of mitochondrial function, including respiratory kinetic characteristics [46]. As shown in these studies, permeabilized cell techniques are powerful methods to investigate enzyme kinetics under natural cellular conditions. However, small molecules may be lost from permeabilized cells, and for cells that have a thick cell wall, strong detergent for permeabilization must be applied, so an intact state is not always maintained.

Even if in vivo kinetics of an enzyme could be successfully captured by these in situ systems, determining the factors that influence activity is required for more detailed modeling. This is not an easy task, but recent progress in metabolomics [47] and proteomics [48] may contribute to discovering trace elements that affect to target enzyme activity. Soga et al. developed capillary electrophoresis mass spectrometry (CE-MS) for metabolome analysis, which permitted detection of 1692 metabolites from *Bacillus subtilis* extracts [49]. Saito et al. applied CE-MS to identify substrates and products of YbhA and YbiV, which were uncharacterized proteins in *E. coli* [50]. de Godoy et al. used reversed-phase nano-scale liquid chromatography (LC) coupled to tandem mass spectrometry (MS/MS) for proteome analysis of yeast, and 2003 proteins were identified in a single experiment [51]. Performance of equipment for metabolomics and proteomics are being steadily improved, allowing detection and quantification of smaller amounts of metabolites and proteins. Currently, however, efficient sample preparation, including rapid quenching of metabolism and good recovery extraction, strongly depend on empirical rules.

Each technique outlined includes specific limitations or is still under development. Thus, further improvements in these techniques and the development of novel techniques to obtain kinetic parameter values that approximate in vivo systems are essential for future dynamic simulations of metabolism. As stressed repeatedly, creating such cell mimic systems is not straightforward; however, we believe our study provides a foundation for the efforts to develop such systems.

Acknowledgements: The authors thank Tomoya Baba, Kenji Nakahigashi, and Yoichi Nakayama for insightful discussions. The authors also thank Tadashi Ogawa for experimental instructions. This study was conducted as part of a Project for Development of a Technological Infrastructure for Industrial Bioprocesses on R&D of New Industrial Science and Technology Frontiers of the Ministry of Economy, Trade, & Industry of Japan (METI), and by the New Energy and Industrial Technology Development Organization (NEDO). This work also was made possible by research funds from the Yamagata Prefectural Government and Tsuruoka City.

Appendix A. Supplementary data

Supplementary data associated with this article can be found, in the online version, at doi:10.1016/j.febslet.2006.12.049.

References

[1] Teusink, B., Passarge, J., Reijenga, C.A., Esgalhado, E., van der Weijden, C.C., Schepper, M., Walsh, M.C., Bakker, B.M., van Dam, K., Westerhoff, H.V. and Snoep, J.L. (2000) Can yeast glycolysis be understood in terms of *in vitro* kinetics of the constituent enzymes? Testing biochemistry. Eur. J. Biochem. 267, 5313–5329.
[2] Smid, E.J., Molenaar, D., Hugenholtz, J., de Vos, W.M. and Teusink, B. (2005) Functional ingredient production: application of global metabolic models. Curr. Opin. Biotechnol. 16, 190–197.
[3] Frieden, C. (1971) Protein–protein interaction and enzymatic activity. Annu. Rev. Biochem. 40, 653–696.
[4] Winkel, B.S. (2004) Metabolic channeling in plants. Annu. Rev. Plant. Biol. 55, 85–107.
[5] Chassagnole, C., Fell, D.A., Rais, B., Kudla, B. and Mazat, J.P. (2001) Control of the threonine-synthesis pathway in *Escherichia coli*: a theoretical and experimental approach. Biochem. J. 356, 433–444.

[6] Rizzi, M., Baltes, M., Theobald, U. and Reuss, M. (1997) *In vivo* analysis of metabolic dynamics in *Saccharomyces cerevisiae*. II. Mathematical model. Biotechnol. Bioeng. 55, 592–608.
[7] Chassagnole, C., Noisommit-Rizzi, N., Schmid, J.W., Mauch, K. and Reuss, M. (2002) Dynamic modeling of the central carbon metabolism of *Escherichia coli*. Biotechnol. Bioeng. 79, 53–73.
[8] Hernandez-Bermejo, B., Fairen, V. and Sorribas, A. (2000) Power-law modeling based on least-squares criteria: consequences for system analysis and simulation. Math. Biosci. 167, 87–107.
[9] Heijnen, J.J. (2005) Approximative kinetic formats used in metabolic network modeling. Biotechnol. Bioeng. 91, 534–545.
[10] Fievet, J.B., Dillmann, C., Curien, G. and de Vienne, D. (2006) Simplified modelling of metabolic pathways for flux prediction and optimization: lessons from an *in vitro* reconstruction of the upper part of glycolysis. Biochem. J. 396, 317–326.
[11] Okino, M.S. and Mavrovouniotis, M.L. (1998) Simplification of mathematical models of chemical reaction systems. Chem.Rev. 98, 391–408.
[12] Blanch, H.W. (1981) Invited review microbial growth kinetics. Chem. Eng. Commun. 8, 181–211.
[13] Alvarez-Vasquez, F., Sims, K.J., Cowart, L.A., Okamoto, Y., Voit, E.O. and Hannun, Y.A. (2005) Simulation and validation of modelled sphingolipid metabolism in *Saccharomyces cerevisiae*. Nature 433, 425–430.
[14] Lall, R. and Voit, E.O. (2005) Parameter estimation in modulated, unbranched reaction chains within biochemical systems. Comput. Biol. Chem. 29, 309–318.
[15] Kitagawa, M., Ara, T., Arifuzzaman, M., Ioka-Nakamichi, T., Inamoto, E., Toyonaga, H. and Mori, H. (2005) Complete set of ORF clones of *Escherichia coli* ASKA library (A Complete Set of *E. coli* K-12 ORF Archive): unique resources for biological research. DNA Res. 12, 291–299.
[16] Marquardt, D. (1963) An algorithm for least-squares estimation of nonlinear parameters. SIAM J. Appl. Math. 11, 431–441.
[17] Dormand, J.R. and Prince, P.J. (1980) A family of embedded Runge–Kutta formulae. J. Comput. Appl. Math. 6, 19–26.
[18] Schmitt, L.M. (2001) Theory of genetic algorithms. Theor. Comput. Sci. 259, 1–61.
[19] Schomburg, I., Chang, A. and Schomburg, D. (2002) BRENDA, enzyme data and metabolic information. Nucleic Acids Res. 30, 47–49.
[20] Alberty, R.A. (2006) Biochemical thermodynamics: applications of Mathematica. Meth. Biochem. Anal. 48, 1–458.
[21] Segel, I.H. (1976) Biochemical Calculations, 2nd ed, John Wiley & Sons Inc., Hoboken, NJ.
[22] Monod, J., Wyman, J. and Changeux, J.P. (1965) On the nature of allosteric transitions: a plausible model. J. Mol. Biol. 12, 88–118.
[23] Blangy, D., Buc, H. and Monod, J. (1968) Kinetics of the allosteric interactions of phosphofructokinase from *Escherichia coli*. J. Mol. Biol. 31, 13–35.
[24] Scopes, R.K. (1973) Studies with a reconstituted muscle glycolytic system. The rate and extent of creatine phosphorylation by anaerobic glycolysis. Biochem. J. 134, 197–208.
[25] Scopes, R.K. (1974) Studies with a reconstituted muscle glycolytic system. The rate and extent of glycolysis in simulated post-mortem conditions. Biochem. J. 142, 79–86.
[26] Itoh, A., Ohashi, Y., Soga, T., Mori, H., Nishioka, T. and Tomita, M. (2004) Application of capillary electrophoresis-mass spectrometry to synthetic *in vitro* glycolysis studies. Electrophoresis 25, 1996–2002.
[27] Cuebas, D. and Schulz, H. (1982) Evidence for a modified pathway of linoleate degradation. Metabolism of 2,4-decadienoyl coenzyme A. J. Biol. Chem. 257, 14140–14144.
[28] Lambeth, M.J., Kushmerick, M.J., Marcinek, D.J. and Conley, K.E. (2002) Basal glycogenolysis in mouse skeletal muscle: *in vitro* model predicts *in vivo* fluxes. Mol. Biol. Rep. 29, 135–139.
[29] Vinnakota, K., Kemp, M.L. and Kushmerick, M.J. (2006) Dynamics of muscle glycogenolysis modeled with pH time course computation and pH-dependent reaction equilibria and enzyme kinetics. Biophys. J. 91, 1264–1287.
[30] Curien, G., Ravanel, S. and Dumas, R. (2003) A kinetic model of the branch-point between the methionine and threonine biosynthesis pathways in *Arabidopsis thaliana*. Eur. J. Biochem. 270, 4615–4627.
[31] Maskow, T. and von Stockar, U. (2005) How reliable are thermodynamic feasibility statements of biochemical pathways? Biotechnol. Bioeng. 92, 223–230.
[32] Spitzer, J.J. and Poolman, B. (2005) Electrochemical structure of the crowded cytoplasm. Trends Biochem. Sci. 30, 536–541.
[33] Dietz, K.J. (2003) Redox control, redox signaling, and redox homeostasis in plant cells. Int. Rev. Cytol. 228, 141–193.
[34] Savageau, M.A. (1995) Michaelis–Menten mechanism reconsidered: implications of fractal kinetics. J. Theor. Biol. 176, 115–124.
[35] Grima, R. and Schnell, S. (2006) A systematic investigation of the rate laws valid in intracellular environments. Biophys. Chem. 124, 1–10.
[36] Minton, A.P. (2006) How can biochemical reactions within cells differ from those in test tubes? J. Cell. Sci. 119, 2863–2869.
[37] Schnell, S. and Turner, T.E. (2004) Reaction kinetics in intracellular environments with macromolecular crowding: simulations and rate laws. Prog. Biophys. Mol. Biol. 85, 235–260.
[38] Derham, B.K. and Harding, J.J. (2006) The effect of the presence of globular proteins and elongated polymers on enzyme activity. Biochim. Biophys. Acta. 1764, 1000–1006.
[39] Rohwer, J.M., Postma, P.W., Kholodenko, B.N. and Westerhoff, H.V. (1998) Implications of macromolecular crowding for signal transduction and metabolite channeling. Proc. Natl. Acad. Sci. USA 95, 10547–10552.
[40] Marchal, D., Pantigny, J., Laval, J.M., Moiroux, J. and Bourdillon, C. (2001) Rate constants in two dimensions of electron transfer between pyruvate oxidase, a membrane enzyme, and ubiquinone (coenzyme Q8), its water-insoluble electron carrier. Biochemistry 40, 1248–1256.
[41] Wong, J.Y., Majewski, J., Seitz, M., Park, C.K., Israelachvili, J.N. and Smith, G.S. (1999) Polymer-cushioned bilayers. I. A structural study of various preparation methods using neutron reflectometry. Biophys. J. 77, 1445–1457.
[42] Korzeniewski, B. (1998) Regulation of ATP supply during muscle contraction: theoretical studies. Biochem. J. 330 (Pt 3), 1189–1195.
[43] Felix, H. (1982) Permeabilized cells. Anal. Biochem. 120, 211–234.
[44] Yoshino, M. and Murakami, K. (1981) *In situ* studies on AMP deaminase as a control system of the adenylate energy charge in yeasts. Biochim. Biophys. Acta. 672, 16–20.
[45] Merkler, D.J., Wali, A.S., Taylor, J. and Schramm, V.L. (1989) AMP deaminase from yeast. Role in AMP degradation, large-scale purification, and properties of the native and proteolyzed enzyme. J. Biol. Chem. 264, 21422–21430.
[46] Saks, V.A. et al. (1998) Permeabilized cell and skinned fiber techniques in studies of mitochondrial function *in vivo*. Mol. Cell. Biochem. 184, 81–100.
[47] Dunn, W.B., Bailey, N.J. and Johnson, H.E. (2005) Measuring the metabolome: current analytical technologies. Analyst 130, 606–625.
[48] Ishihama, Y. (2005) Proteomic LC–MS systems using nanoscale liquid chromatography with tandem mass spectrometry. J. Chromatogr. A 1067, 73–83.
[49] Soga, T., Ueno, Y., Naraoka, H., Ohashi, Y., Tomita, M. and Nishioka, T. (2002) Simultaneous determination of anionic intermediates for *Bacillus subtilis* metabolic pathways by capillary electrophoresis electrospray ionization mass spectrometry. Anal. Chem. 74, 2233–2239.
[50] Saito, N., Robert, M., Kitamura, S., Baran, R., Soga, T., Mori, H., Nishioka, T. and Tomita, M. (2006) Metabolomics approach for enzyme discovery. J. Proteome. Res. 5, 1979–1987.
[51] de Godoy, L.M., Olsen, J.V., de Souza, G.A., Li, G., Mortensen, P. and Mann, M. (2006) Status of complete proteome analysis by mass spectrometry: SILAC labeled yeast as a model system. Genome Biol. 7, R50.
[52] Johnson, J.L. and Reinhart, G.D. (1992) MgATP and fructose 6-phosphate interactions with phosphofructokinase from *Escherichia coli*. Biochemistry 31, 11510–11518.